# Predictive Capabilities of Turbulence Models for a Confined Swirling Flow

Yong G. Lai*

*CFD Research Corporation,
Huntsville, Alabama 35805*

## Introduction

**S**WIRLING flows are commonly encountered in many types of combustion devices such as furnaces, gas turbines, and ram-jet engines. Accurate predictions of such flows are critical in the design of advanced propulsion systems. In the past, a significant amount of computational work has been reported using the eddy-viscosity turbulence models.[1-3] Relatively speaking, however, only a few studies have been carried out using the Reynolds stress transport turbulence model (designated as RST model in the remaining of this paper). Among them is the work by Hogg and Leschziner[4] and Jones and Pascau.[5] Both studies calculated swirling flows for which no centerline flow reversal was present.

In this study, the predictive capability of the RST turbulence model[6] is investigated for a confined swirling flow with the presence of a swirl-induced flow reversal at the centerline. For comparative purposes, the renormalization group (RNG)-based $K-\varepsilon$ model[7] is also examined and compared with the standard $K-\varepsilon$ model.[8] The selected swirling flow was experimentally studied by Nejad et al.[9] The case is quite suitable for the purpose of turbulence model assessment since a complete set of mean velocity and Reynolds stress components is available near the swirl discharge plane of the combustion chamber. Therefore, no ambiguity exists in determining the inlet boundary conditions.

## Turbulence Models and Numerical Methods

This study considers two-dimensional axisymmetric configurations with steady and incompressible assumptions. Therefore, the ensemble-averaged Navier–Stokes equations as reported in Refs. 4 and 5 are used. Basically, the Reynolds stress components are unknowns, and they need to be provided with suitable turbulence models. Three turbulence models are used in this study. They are the standard $K-\varepsilon$ model of Launder and Spalding,[8] the RNG-based $K-\varepsilon$ model of Yakhot et al.[7] and the RST model of Gibson and Launder.[6] Detailed equations for these models are readily available from Refs. 7–9 and will not be presented here.

The mass, momentum, and turbulence transport equations are solved numerically using a finite volume pressure-based computational fluid dynamics (CFD) method with collocated grid arrangement. The pressure and mean velocity coupling are resolved with the SIMPLEC algorithm,[10] and the convective terms are discretized with the second-order upwind scheme. The numerical method with the eddy-viscosity turbulence model is quite standard, and a detailed discretization and solution procedure can be found in Ref. 11. For the RST turbulence model, two prominent numerical issues need to be resolved. One issue arises as no apparent turbulent viscosity is available in the momentum equations. Another is the potential numerical oscillations created with the collocated grid arrangement of Reynolds stresses. In this study, the approach of Lai[12] is used and extended for swirling flow calculations. This approach will not only provide turbulent diffusionlike terms in the momentum equations but also prevent the numerical oscillations from happening. A detailed presentation of the approach may be found in Ref. 12 and will not be repeated here.

## Computational Results

### Computational Details

The geometry of the confined swirling flow is depicted in Fig. 1. The dump combustor consists of two sections: the inlet pipe and the combustion chamber. The inlet pipe has an inner diameter of 101.6 mm and the dump plane is located at $x/h = 0.0$ ($h$ is the step height). The combustion chamber has a length of 1850 mm and an inner diameter of 152.4 mm. Air is the working fluid and the inlet centerline velocity is maintained at 19.2 m/s. The Reynolds number based on the combustion chamber diameter and the inlet centerline velocity is $1.25 \times 10^5$. The computation corresponds to the case with a swirl number of 0.5. The swirl number is defined as

$$S = \int_{R_h}^{R_i} UWr^2 \, dr \bigg/ \int_{R_h}^{R_i} R_i U^2 r \, dr$$

where $U$ and $W$ are the mean axial and swirl velocities, $R_h$ and $R_i$ are the swirler hub and inlet pipe radius, and $r$ is the radial coordinate.

The inlet of the computational domain is located at $x/h = 0.38$ where detailed experimental data are available (three velocity and six Reynolds stress components). The only uncertainty at the inlet is the specification of the turbulent dissipation rate $\varepsilon$. In this study, the $\varepsilon$ is estimated with the turbulence energy equilibrium assumption, i.e., $\varepsilon = K^{1.5}/(\alpha R)$, where $R$ is the combustion chamber radius and $\alpha$ is a constant. In previous studies,[4,13] the value of $\alpha$ ranged from 0.3 to 0.36. In this paper, an extensive sensitivity study has been carried out and it is determined that $\alpha = 0.36$ is an adequate and physically sound selection.

The outlet boundary of the computational domain is placed at $x/h = 72.8$ and all main variables are extrapolated. This is achieved by setting the first derivatives of all main variables to zero. At solid walls, the implementation of the boundary conditions is derived from the standard wall function approach[8,12] to avoid a detailed near-wall treatment. At the centerline, the derivatives of all variables are set to zero except for the Reynolds shear stress components $\tau_{xr}$ and $\tau_{r\theta}$. Instead, they are set to zero at the centerline. In the preceding, $x, r$, and $\theta$ are the axial, radial, and circumferential coordinates, respectively.

A careful grid independence study has been performed and the results suggested that a 120 × 60 (axial and radial) grid was adequate for the present computation. This grid is highly nonuniform in both directions. In the axial direction, 30 cells are uniformly spaced between $x/h = 0.38$ (inlet) and 4, whereas 60 cells are nonuniformly distributed from $x/h = 4$ to 26. In the radial direction, the first grid point near a wall is placed such that $y+$, the wall coordinate defined with wall distance and friction velocity, ranges from 30 to 60.

### Results and Discussion

The calculated streamline patterns of the three turbulence models are displayed in Fig. 2, and the predicted sizes of the central separation zone and the corner reattachment length are also marked in the figure. The experimental measurement[9] showed that the central separation zone had a size of $4.4h$ whereas the reattachment length was $3.2h$. It is seen that the RST model clearly predicts the occurrence of the central reversed zone. However, the size is overpredicted and this overprediction may be attributed to the pressure-strain model, which has been widely known to be the weak part of a RST model. On the other hand, both the standard $K-\varepsilon$ and RNG-based $K-\varepsilon$ models fail to predict the existence of the central reversed zone. It is believed that this failure results from the isotropic eddy-viscosity
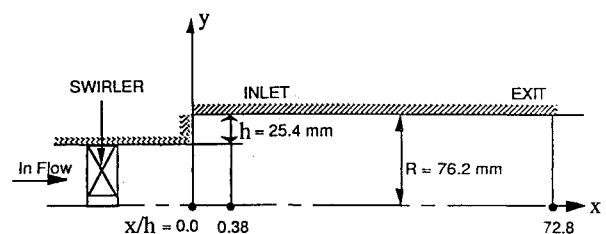


**Fig. 1 Geometry of the swirling flow.**

assumption. The isotropy leads to a too-high turbulence viscosity for swirling flows and consequently suppresses the central reversed zone.

To substantiate the preceding argument, the flow is recalculated using the standard $K-\varepsilon$ model with much lower inlet turbulent viscosity. It is achieved by increasing the inlet turbulence dissipation rate $\varepsilon$ by a factor of 5. It is found that the central reversed flow will appear. As expected, however, the calculated turbulence kinetic energy deviates too far from the experimental data near the inlet ($x/h = 1.0$). Thus the elevated $\varepsilon$ is not justifiable.

The prediction of the corner recirculation zone is less sensitive to the inlet conditions. Overall, the RST model provides the best agreement to the measured data for the corner reattachment length. It is seen that both eddy-viscosity models overpredicted the reattachment length, a behavior contrary to the case of a sudden expansion flow without swirl. Experimentally, it was found that the reattachment length was decreased from $8.0h$ for the zero-swirl case to $3.2h$ for the 0.5 swirl number case.[9] The decrease for the swirling flow is caused by the rapid expansion of the flow induced by the



Fig. 2    Calculated streamline plots: a) Reynolds stress transport model, b) standard $K-\varepsilon$ model, and c) RNG-based $K-\varepsilon$ model.

swirl-created centrifugal force. Therefore, it suggests that the eddy-viscosity models fail to properly take into account the action of swirl generated centrifugal force. It should be pointed out, in passing, that the RNG-based $K-\varepsilon$ model consistently predicts a larger corner recirculation than the standard $K-\varepsilon$ model (with or without swirl). If no swirl is present, the RNG model tends to have a much better prediction of the reattachment length than the standard $K-\varepsilon$ model (see Speziale and Thangam[14]). For swirling flows, however, the RNG model can predict worse results than the standard $K-\varepsilon$ model, as is evident in this study.

Comparisons of the calculated and measured radial variations of the mean axial velocity, swirl velocity, and the turbulence kinetic energy are shown in Fig. 3 at several axial locations. Again, the RST model is found to give the best overall agreement with the measured data. The differences between the standard and RNG-based $K-\varepsilon$ models are not significant. For the mean axial velocity, the major difference among different models is confined to the central separation zone. The most noteworthy difference of results among different models is the prediction of the mean swirl velocity downstream of the dump plane ($x/h = 5.0$). As is clear in Fig. 3b, the two eddy-viscosity models predict that the swirling flow will eventually approach a solid-body-rotational type. This solid-body-rotational flow will remain until the end of the calculation domain (this is the reason $x/h = 18.0$ is added to Fig. 3b). However, the experimental data suggested that the flow retained the strength of its vortex core all of the way to the exit and did not evolve into a solid-body-rotational flow. This interesting feature is only present at high swirl numbers[9] and is captured well by the RST model. The preceding results indicate that the RST model is capable of accounting for the complex interactions between swirl and the turbulence field.

The turbulence kinetic energy is predicted well by all models near the inlet ($x/h = 1.0$) as seen in Fig. 3c. But further downstream, the eddy-viscosity models predict much lower turbulence kinetic energy levels. This underprediction is probably responsible for the failure of the models to preserve the strength of the vortex core. The RST model provides better agreement with the data. However, larger discrepancies could be noticed particularly around $x/h = 5.0$ and near the centerline. The underprediction of $K$ around $x/h = 5.0$ is probably responsible for the overprediction of the central separation zone. With the limited information available, no definite conclusion can be drawn with regard to this discrepancy.

## References

[1]Sturgess, G. J., and Syed, S. A., "Calculation of Confined Swirling Flows," AIAA Paper 85-0060, Jan. 1985.

[2]Rhode, D. L., and Stowers, S. T., "Turbulence Model Assessment for Confined Mixing of Co-Swirling Concentric Jets," AIAA Paper 85-1269, July 1985.



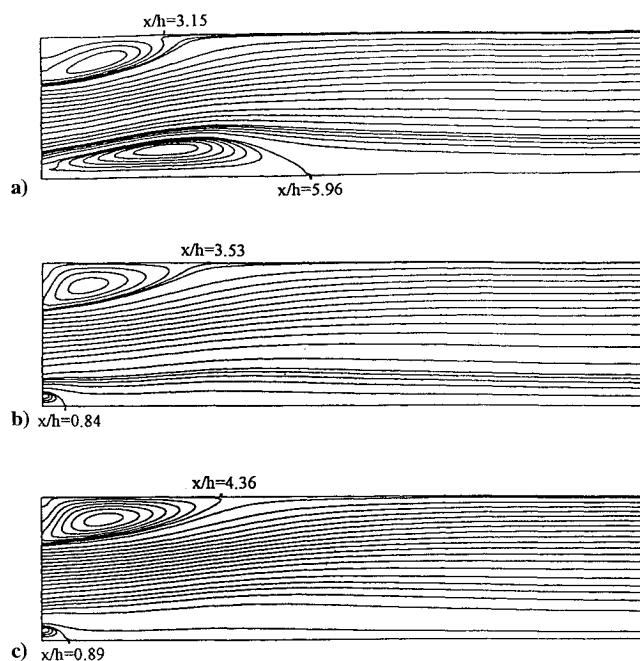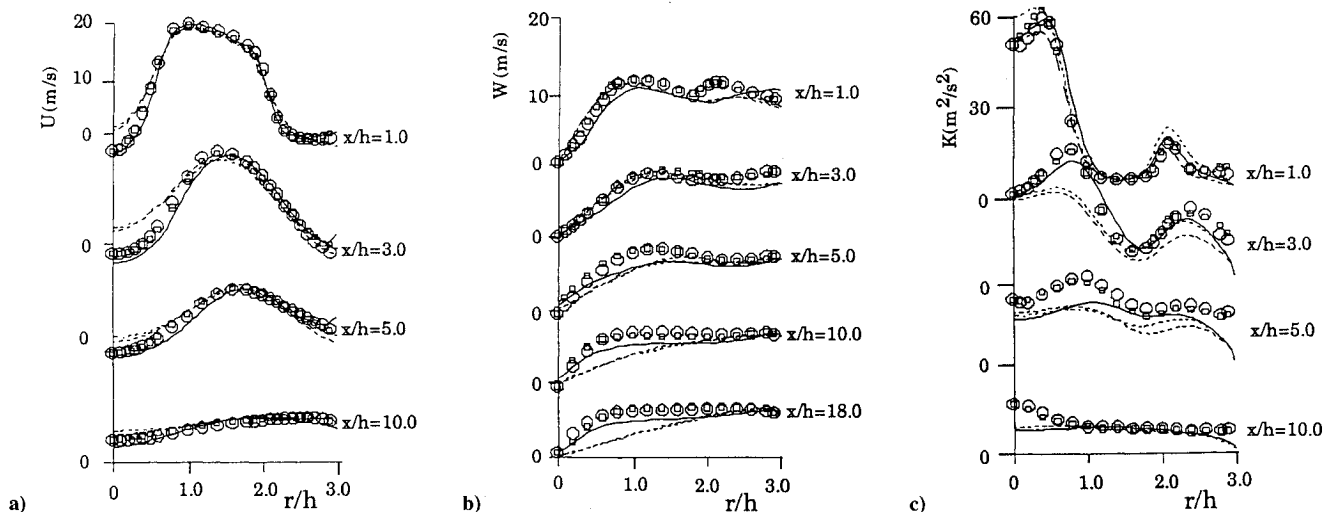Fig. 3    Comparison of calculated and measured mean variable (two symbols in the measured data represent two sets of measurements): a) mean axial velocity, b) mean swirl velocity, and c) turbulent kinetic energy. ○ □, experimental data; ———, RST model; - - - -, $K-\varepsilon$ model; and – – –, RNG model.

[3]Srinivasan, R., and Mongia, H. C., "Numerical Computation of Swirling Recirculating Flows," NASA CR 165197, Sept. 1980.

[4]Hogg, S., and Leschziner, M. A., "Computation of Highly Swirling Confined Flow with a Reynolds Stress Turbulence Model," *AIAA Journal*, Vol. 27, No. 1, 1989, pp. 57–63.

[5]Jones, W. P., and Pascau, A., "Calculation of Confined Swirling Flows with a Second Moment Closure," *Journal of Fluids Engineering*, Vol. 111, Sept. 1989, pp. 248–255.

[6]Gibson, M. M., and Launder, B. E., "Ground Effects on Pressure Fluctuations in the Atmospheric Boundary Layer," *Journal of Fluid Mechanics*, Vol. 86, April 1978, pp. 491–511.

[7]Yakhot, V., Orszag, S. A., Thangam, S., Gatski, T. B., and Speziale, C. G., "Development of Turbulence Models for Shear Flows by a Double Expansion Technique," *Physics of Fluids A*, Vol. 4, No. 7, 1992, pp. 1510–1520.

[8]Launder, B. E., and Spalding, D. B., "The Numerical Computation of Turbulent Flows," *Computer Methods in Applied Mechanics and Engineering*, Vol. 3, May 1974, pp. 269–289.

[9]Nejad, A. S., Favaloro, S. C., Vanka, S. P., Samimy, M., and Langenfeld. C., "Application of Laser Velocimetry for Characteristics of Confined Swirling Flow," *Journal of Engineering for Gas Turbines and Power*, Vol. 111, No. 1, 1989, pp. 36–45.

[10]van Doormal, J. P., and Raithby, G. D., "Enhancement of the SIMPLE Method for Predicting Incompressible Fluid Flows," *Numerical Heat Transfer*, Vol. 7, No. 2, 1984, pp. 147–163.

[11]Lai, Y. G., So, R. M. C., and Przekwas, A. J., "Turbulent Transonic Flow Simulation Using a Pressure-Based Method," *International Journal of Engineering Science*, Vol. 33, No. 4, 1995, pp. 469–483.

[12]Lai, Y. G., "Computational Method of Second-Moment Turbulence Closures in Complex Geometries," *AIAA Journal*, Vol. 33, No. 8, 1995, pp. 1426–1432.

[13]Favaloro, S., Nejad, A., Ahmed, S., Miller, T., and Vanka, S., "An Experimental and Computational Investigation of Isothermal Swirling Flow in an Axisymmetric Dump Combustor," AIAA Paper 89-0620, Jan. 1989.

[14]Speziale, C. G., and Thangam, S., "Analysis of an RNG Based Turbulence Model for Separated Flows," NASA CR 189600, Jan. 1992.

# Ionizational Nonequilibrium Induced by Neutral Chemistry in Air Plasmas

Christophe O. Laux,* Richard J. Gessman,† and
Charles H. Kruger‡
*Stanford University, Stanford, California 94305-3032*

## Introduction

IONIZATIONAL nonequilibrium in plasmas can greatly affect the reactivity, transport properties (thermal and electrical conductivity), and radiative phenomena because of collisional coupling between the populations of bound and free electrons. Normally, departures from equilibrium in the population of free electrons are attributed to either (or both) differences between electron and gas kinetic temperatures or finite ionization/electron recombination rates. In contrast, the computational study reported here for a recombining air plasma suggests that under appropriate circumstances ionizational nonequilibrium may be caused instead by finite dissociation/recombination rates for neutral species. Thus we find the unexpected result that nonequilibrium populations of neutral species can cause ionizational nonequilibrium in molecular plasmas. The

consequences of this effect on the radiative power of NO in air plasmas are examined.

## Model

This study considers ionizational nonequilibrium in a recombining air plasma assumed to be thermal (equal electron and heavy particle temperatures). Although the phenomena described herein are by no means limited to thermal plasmas, they can be described more clearly with a single temperature plasma. The Chemkin solver[1] was used for one-dimensional kinetics modeling with specified initial concentrations and with imposed temperature variations. Three air reaction mechanisms [Dunn and Kang,[2] Gupta et al. (GYTL),[3] and Park[4,5]] were considered. Reverse reaction rates were obtained by detailed balance using the equilibrium thermodynamic properties computed by Liu and Vinokur.[6] The air plasma was assumed to be initially in chemical equilibrium at 7500 K and 1 atm. A linear temperature drop from 7500 to 4500 K within 0.6 ms was then imposed on the plasma, and the concentration evolution of the major neutral and charged species was computed with Chemkin. At each time, concentrations were normalized to their chemical equilibrium values at the corresponding temperature. The resulting normalized concentrations, or nonequilibrium factors, are shown in Fig. 1. Observations derived from these results are discussed in the next section.

To check the thermal plasma assumption, we have calculated the differences between the electron kinetic temperature $T_e$, the gas kinetic temperature $T_h$, and the vibrational temperature $T_v$ and found that they are negligible for the conditions of this Note. For molecular plasmas with no applied external field, the electron energy equation[7] is

$$3n_e \sum_{species\ s} \frac{m_e}{m_s} \bar{\nu}_{es} \delta_s k(T_e - T_h) = \sum_{ion\ i} \varepsilon_i \frac{\partial n_i}{\partial t}\bigg|_{3\ body-recombination} \quad (1)$$

where $n_e$, $m_e$, and $m_s$ represent the electron number density, the electron mass, and the mass of heavy species $s$, respectively; $\delta_s$ is the so-called nonelastic energy loss factor, used as a multiplier to the rate of energy transferred by elastic collisions to model the effect of nonelastic collisions; and the term on the right-hand side represents the net rate of energy transferred to the electrons by three-body ion
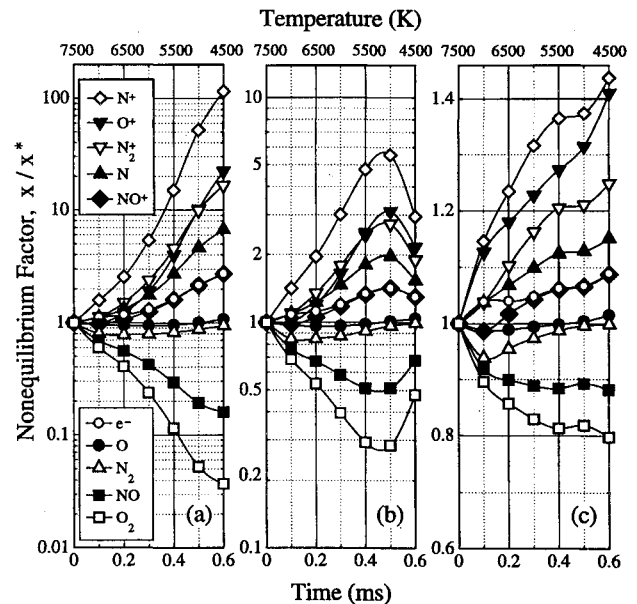


Fig. 1 Nonequilibrium factors predicted with the reaction mechanisms of a) Dunn and Kang, b) GYTL, and c) Park. The validity of Eqs. (2), (4), and (5) for $t > 0.3$ ms can be verified from these figures. For instance, that the electron overpopulation factor varies as the square root of the N overpopulation factor [Eq. (4)] can be seen most easily in the logarithmic plots (a and b), where the electron overpopulation curve lies half the distance from the equilibrium line ($x/x^* = 1$) to the N overpopulation curve.